Analyst

PAPER

View Article Online
View Journal | View Issue



Cite this: *Analyst*, 2020, **145**, 7736

# A cytosolically localized far-red to near-infrared rhodamine-based fluorescent probe for calcium ions†

Koji Numasawa,[a] Kenjiro Hanaoka, *[a] Takayuki Ikeno,[a] Honami Echizen,[a] Tomoe Ishikawa,[a] Masakazu Morimoto,[b] Toru Komatsu,[a] Tasuku Ueno,[a] Yuji Ikegaya,[a] Tetsuo Nagano[c] and Yasuteru Urano*[a,d,e]

Received 31st August 2020,
Accepted 22nd September 2020

DOI: 10.1039/d0an01739f

rsc.li/analyst

$Ca^{2+}$ is one of the most important second messengers in cells. A far-red to near-infrared (NIR) $Ca^{2+}$ fluorescent probe is useful for multi-color imaging in GFP or YFP-expressing biosamples. Here we developed a cytosolically localized far-red to NIR rhodamine-based fluorescent probe for $Ca^{2+}$, **CaSiR-2 AM**, while rhodamine dyes are basically localized to mitochondria or lysosomes in cells.



$Ca^{2+}$ is one of the most important second messengers inside cells, and concentration changes of intracellular $Ca^{2+}$ are involved in various biological phenomena.[1,2] Visualization of intracellular $Ca^{2+}$ is important for mechanistic studies of these processes, and fluorescence imaging with $Ca^{2+}$ indicators is a widely used method.[3,4] Fluorescent indicators for $Ca^{2+}$ can be categorized into two classes: genetically encoded fluorescent protein-based $Ca^{2+}$ sensors, and small organic fluorescent molecule-based $Ca^{2+}$ sensors.[5–7] Although both types have specific advantages and drawbacks, small-molecular organic fluorescent probes are convenient, because they can be loaded into cells without transfection and generally possess better photophysical properties, such as high brightness and high photostability, than fluorescent proteins.[8]

Currently, green-emitting fluorescent probes for $Ca^{2+}$, such as Fluo-3,[9] Fluo-4,[10] Calcium Green-1,[11] and Oregon Green 488 BAPTA-1,[12] are widely used in biological studies. More recently, some fluorescent probes emitting in the far-red to NIR (650–900 nm) region have been developed,[7] and these are useful for multicolor imaging in combination with UV- to yellow-emitting fluorescent indicators. Far-red to NIR light penetrates deeper into tissues than UV to red light does; in addition there is less background autofluorescence in this region, and phototoxicity is reduced.[13,14] Since the visualization of cytoplasmic $Ca^{2+}$ is important for biological studies, several fluorescein analogue-based fluorescent probes that distribute to the cytosol in cells, probably due to their inherent negative charge, have been developed and used for live-cell fluorescence imaging.[15–17] On the other hand, rhodamine is a well-known biocompatible dye scaffold with high fluorescence quantum yield ($\Phi_{fl}$) and high water solubility, and also possess longer absorption and emission wavelengths covering the red to NIR region, as well as higher photostability than fluorescein analogues.[18] There are some established rhodamine-based red-emitting fluorescent probes for $Ca^{2+}$, such as Rhod-2 AM.[9] This red fluorescent probe is widely used for biological studies, but the cationic nature of the rhodamine scaffold causes Rhod-2 AM to localized in mitochondria.[15] We also developed a Si-rhodamine(SiR)-based NIR fluorescent probe for $Ca^{2+}$, **CaSiR-1 AM** (Fig. S1†).[19] This probe exhibited absorption and emission ($\lambda_{abs}/\lambda_{em}$ = 650/664 nm) in the far-red to NIR region, and its activation ratio in response to $Ca^{2+}$ was very high (>1000). Furthermore, it could be used simultaneously with green to red fluorescent fluorophores such as GFP, Venus and sulforhodamine 101 for neuronal imaging,[19,20] however, we found that it showed poor reproducibility in experiments with mouse brain slices. We considered that this problem was likely due to its localization into organelles in living cells.[15] So, we set out to develop a far-red to NIR-emitting, rhodamine-based fluorescent probe for $Ca^{2+}$ that would be retained in the cytosol in living cells, though the cytosolic localization of rhodamine dyes is considered to be highly challenging.

As a first step, we considered the molecular requirements for Si-rhodamine dyes to distribute in the cytoplasm. We focused on the 2-COOH SiR650 scaffold (Fig. 1a), because

[a]*Graduate School of Pharmaceutical Sciences, The University of Tokyo, 7-3-1 Hongo, Bunkyo-ku, Tokyo 113-0033, Japan. E-mail: uranokun@mol.f.u-tokyo.ac.jp, khanaoka@mol.f.u-tokyo.ac.jp*
[b]*Department of Chemistry and Research Center for Smart Molecules, Rikkyo University, 3-34-1 Nishi-Ikebukuro, Toshima-ku, Tokyo 171-8501, Japan*
[c]*Drug Discovery Initiative, The University of Tokyo, 7-3-1 Hongo, Bunkyo-ku, Tokyo 113-0033, Japan*
[d]*Graduate School of Medicine, The University of Tokyo, 7-3-1 Hongo, Bunkyo-ku, Tokyo 113-0033, Japan*
[e]*CREST (Japan) Agency for Medical Research and Development (AMED), 1-7-1 Otemachi, Chiyoda-ku, Tokyo 100-0004, Japan*
†Electronic supplementary information (ESI) available: Synthesis, protocols, characterization and spectra. See DOI: 10.1039/d0an01739f

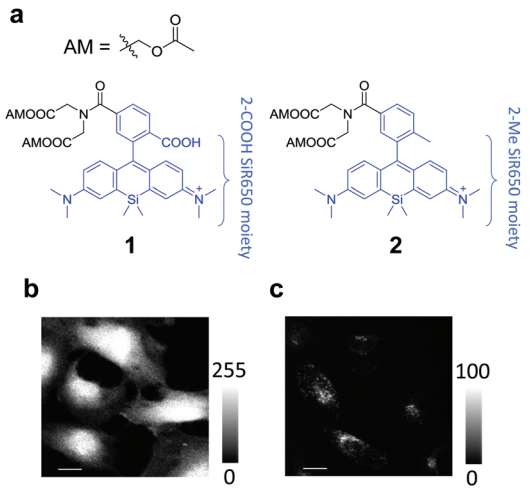


**Fig. 1** (a) Structures of the synthesized cytosolically retained Si-rhodamine dye **1** and its control dye **2**. (b and c) Fluorescence images of HeLa cells incubated with 1 μM **1** (b) or **2** (c) for 1 h. Ex. 650 nm; Em. 670–750 nm. Scale bar: 20 μm.

Weissleder's group recently reported that its labelled ligands did not show non-targeted localization inside living cells in fluorescence imaging.[21–23] Moreover, since the mitochondrial or lysosomal localization of rhodamine dyes is probably due to their cationic charge and hydrophobicity, we hypothesized that the introduction of a carboxy group into the Si-rhodamine scaffold to change the net charge from +1 to 0, making the dye more hydrophilic, is effective to promote cytoplasmic accumulation.

Based on the above hypothesis, we designed and synthesized a Si-rhodamine dye **1** bearing a cytosol-retaining moiety, *i.e.*, this dye consists of the 2-COOH SiR650 moiety, which may have no intrinsic intracellular localization ability to specific organelles, together with the iminodiacetic acid moiety as a cytosol-retaining moiety (Fig. 1a). We also expected that this scaffold possesses a cell-membrane permeability because of the easy formation of the spirolactone form of 2-COOH SiR650 as previously reported.[24,25] We also observed the intramolecular spirolactone form of 2-COOH SiR650 by single-crystal X-ray analysis (Fig. S2†). We then synthesized a control dye **2**, consisting of 2-Me SiR650 and the iminodiacetic acid moiety (Fig. 1a). The carboxy groups of the iminodiacetic acid moiety were masked with acetoxymethyl (AM) groups to make the compounds cell-membrane-permeable as shown in Fig. S3.† We also examined the photophysical properties of the unprotected forms of **1** and **2**, and found that these compounds showed almost the same photophysical properties (Fig. S4†). We then used **1** and **2** for live-cell fluorescence imaging. As a result, **1** was distributed to the cytoplasm and nucleus, but not mitochondria or lysosomes, as expected (Fig. 1b). On the other hand, when we applied **2** to live-cell fluorescence imaging, the dye distributed to lysosomes (Fig. 1c and Fig. S5†). These results confirm the validity of our design strategy of combining the 2-COOH SiR650 moiety and a cytosol-retaining moiety having plural carboxy groups in order to obtain a cytosolically distributed Si-rhodamine dye.

Based on the above results, we set out to develop a cytosolically retained NIR fluorescent probe for $Ca^{2+}$ by utilizing the 2-COOH SiR650 scaffold. We employed the BAPTA derivative as a $Ca^{2+}$-chelating moiety. Since the BAPTA moiety works as not only a $Ca^{2+}$-chelating moiety, but also an electron-donating moiety for photoinduced electron transfer (PeT) to the fluorophore moiety,[15,19] the distance between the BAPTA derivative and the fluorophore moiety is important to control the fluorescence intensity change of the fluorescent probe in the presence of $Ca^{2+}$. So, we designed and synthesized three candidates as fluorescent probes for $Ca^{2+}$ by introducing the BAPTA derivative at different positions of the 2-COOH SiR650 dye scaffold (Fig. 2a and Fig. S6†). In this molecular design, we expected that the BAPTA derivative would also work as a cytosol-retaining moiety, as well as the iminodiacetic acid moiety of **1**. We examined the absorbance and fluorescence changes of these candidates in the presence of various concentrations of free $Ca^{2+}$, and also determined their $K_d$ values for $Ca^{2+}$. All probes showed a $Ca^{2+}$-concentration-dependent fluorescence intensity increase, with practical $K_d$ values for $Ca^{2+}$ (Fig. 2b, Fig. S6, S7 and Table S1†). Among the synthesized probes, **CaSiR-2** showed the lowest fluorescence quantum yield in the absence of $Ca^{2+}$, probably due to the efficient PeT process, and the largest fluorescence activation ratio (up to 26). This is probably due to the shortest distance between the BAPTA derivative (the electron-donating moiety) and the fluorophore moiety (the electron-accepting moiety), which pro-

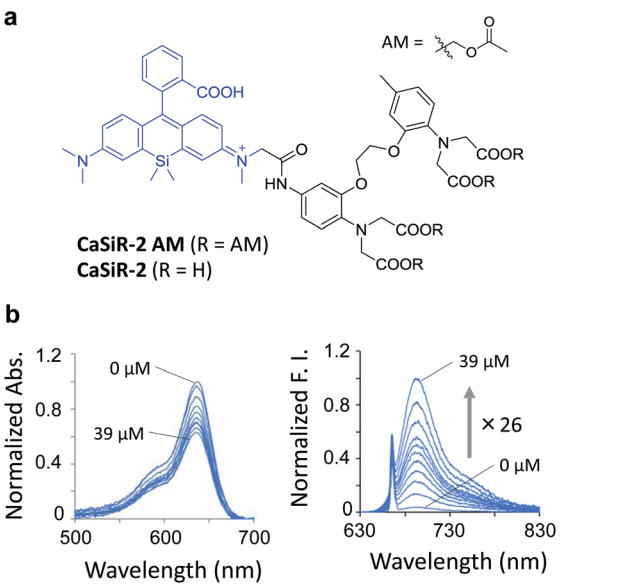


**Fig. 2** (a) Structures of **CaSiR-2** and **CaSiR-2 AM**. (b) Normalized absorption (left) and fluorescence (right) spectra of **CaSiR-2** in the presence of various concentrations of free $Ca^{2+}$ (0, 0.017, 0.038, 0.065, 0.100, 0.150, 0.225, 0.351, 0.602, 1.35, 39 μM) in 30 mM MOPS buffer containing 100 mM KCl and 10 mM EGTA, pH 7.2. The excitation wavelength was 635 nm.

motes the PeT process in the absence of $Ca^{2+}$. Based on these results, we next examined the performance of **CaSiR-2** in biological applications.

For live-cell fluorescence imaging, we synthesized **CaSiR-2 AM** (Fig. 2a), in which the carboxy groups of the BAPTA moiety are protected by AM esters. The AM protecting groups should be removed by intracellular esterases in the same way as shown in Fig. S3.† We incubated HeLa cells with **CaSiR-2 AM** and found that **CaSiR-2** was mostly distributed in the cytosol and nucleus (Fig. 3a). On the other hand, **CaSiR-1** was strongly localized in lysosomes, as previously reported by our group,[15] and strong fluorescence was observed from lysosomes regardless of the stimulation of $Ca^{2+}$ oscillation (Fig. 3a). This is probably because of the high concentration of $Ca^{2+}$ in lysosomes (200–600 μM) compared with that in cytosol.[26]

We then conducted fluorescence imaging of histamine-induced[27] or ATP-induced[28,29] intracellular calcium oscillations in HeLa cells utilizing **CaSiR-2 AM**. Histamine or ATP was applied to the cells at 90 s after the fluorescence imaging was started, then the $Ca^{2+}$ ionophore, ionomycin, was further added at 210 s to increase the intracellular $Ca^{2+}$ concentration (Fig. 3b, c and Fig. S8†). The changes of cytoplasmic $Ca^{2+}$ concentration were clearly visualized by **CaSiR-2 AM** (see ESI Movie 1 for the experiment with histamine stimulation). We also performed the same experiments with **CaSiR-1 AM** for comparison (Fig. 3d, e and Fig. S9†). We found that some cells showed a large background fluorescence increase after stimulation with histamine or ATP compared to the experiments with **CaSiR-2 AM**, though the intracellular $Ca^{2+}$ oscillations could still be observed in some cells. A possible reason for this is that the fluorescence signal of **CaSiR-1** represents the sum of the $Ca^{2+}$ concentration changes in lysosomes and cytoplasm in cells, and the $Ca^{2+}$ concentration in lysosomes might have increased in a constant manner. Moreover, it appeared that **CaSiR-1 AM** was loaded mainly into lysosomes in some cells, but into both lysosomes and cytoplasm in other cells, probably because of the cell condition; such a difference in the loading pattern of the dye would markedly influence the $Ca^{2+}$ responses of individual cells to histamine or ATP stimulation, as shown in Fig. 3e and Fig. S9.†

Finally, we performed fluorescence imaging of $Ca^{2+}$ with **CaSiR-2 AM** or **CaSiR-1 AM** to monitor neuronal activity in rat hippocampal cultured slices. We bulk-loaded **CaSiR-2 AM** or **CaSiR-1 AM** into rat hippocampal neurons, and recorded the spontaneous neuronal activities. As shown in Fig. 4, while **CaSiR-2 AM** was uniformly distributed in the cytosol, **CaSiR-1 AM** showed localization to organelles. This difference of localization pattern between **CaSiR-2 AM** and **CaSiR-1 AM** is consistent with that seen in the live-cell fluorescence imaging (Fig. 3a). Both fluorescent probes could visualize spontaneous neural firing in terms of changes of fluorescence intensity (Fig. 4). However, while **CaSiR-2 AM** showed sharp peaks of fluorescence intensity change with a high S/N ratio (Fig. 4a), the baseline fluorescence intensity of **CaSiR-1 AM** was noisy and the peaks of the fluorescence intensity change were also unclear (Fig. 4b). It is noteworthy that the difference in the intracellular localization of the fluorescent indicators results in a difference in the sharpness of the fluorescence signal. The reason for the poorer performance of **CaSiR-1** is considered to

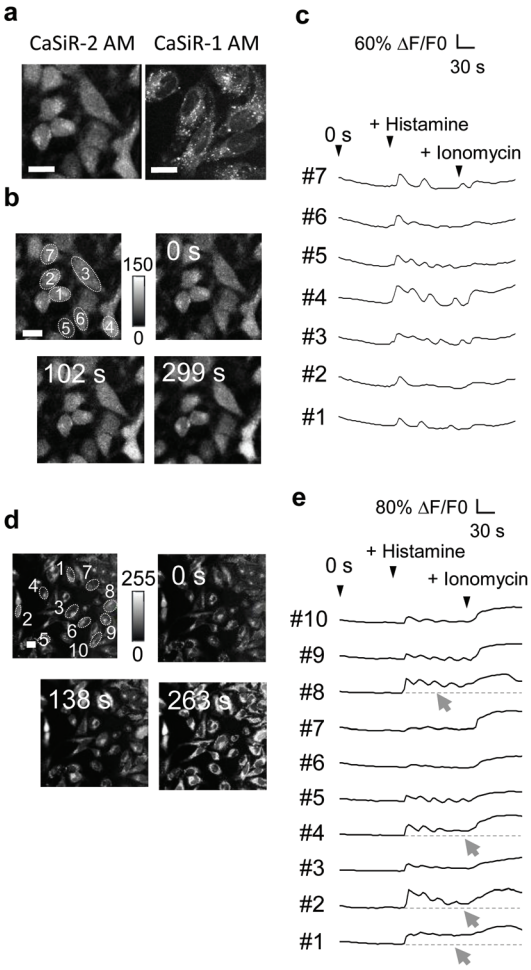


**Fig. 3** (a) Fluorescence images of HeLa cells incubated with 3 μM **CaSiR-2 AM** or **CaSiR-1 AM** in HBSS (Hank's balanced salt solution) containing 0.03% Pluronic and 0.45% DMSO at 37 °C for 30 min. (b and c) Fluorescence imaging of histamine-induced calcium oscillations in HeLa cells utilizing **CaSiR-2 AM**. HeLa cells were incubated with 3 μM **CaSiR-2 AM** in HBSS containing 0.03% Pluronic and 0.45% DMSO as a cosolvent at 37 °C for 30 min. Then, the cells were washed three times, and the fluorescence imaging was started. Cells were stimulated with 1 μM histamine at 90 s and then with 5 μM ionomycin at 210 s. Fluorescence images were taken at the time points indicated in each fluorescence image (b). Fluorescence intensity changes in regions of interest (ROIs) of individual cells numbered 1–7 in (b) are shown in (c). Scale bars: 20 μm. (d and e) Fluorescence imaging of histamine-induced calcium oscillations in HeLa cells utilizing **CaSiR-1 AM**. HeLa cells were incubated with 3 μM **CaSiR-1 AM** in HBSS containing 0.03% Pluronic and 0.45% DMSO as a cosolvent at 37 °C for 30 min. The cells were washed three times, and the fluorescence imaging was started. Cells were stimulated with 1 μM histamine at 90 s and then with 5 μM ionomycin at 210 s. Fluorescence images were taken at the time points indicated in each fluorescence image (d). Fluorescence intensity changes in ROIs of individual cells numbered 1–10 in (d) are shown in (e). Gray arrows indicate the background fluorescence increase after stimulation with histamine. The cell numbered 1 showed an especially clear background fluorescence increase. Scale bars: 20 μm.

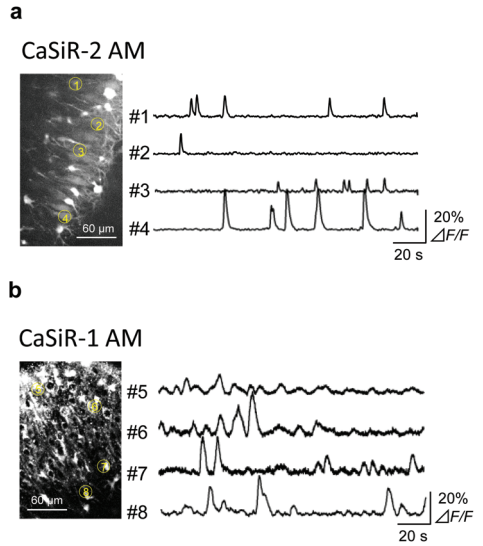


**Fig. 4** Rat hippocampal neurons of a brain slice loaded with **CaSiR-2 AM** (a) or **CaSiR-1 AM** (b). Fluorescence traces of individual cells are shown. Spontaneous action potentials were visualized in each cell, and some of the activities were synchronized across neurons.

be that **CaSiR-1** also responded to $Ca^{2+}$ concentration changes in organelle(s) other than the cytosol.

To examine this issue in more detail, we performed costaining of rat hippocampal slices with **CaSiR-1 AM** and LysoTracker or MitoTracker (Fig. S10a†). We found that the fluorescence of **CaSiR-1 AM** coincided well with that of LysoTracker, but not MitoTracker, indicating that **CaSiR-1 AM** is localized to lysosomes in neurons, as was also the case in the fluorescence imaging of HeLa cells. Further, we recorded the fluorescence intensity changes of **CaSiR-1 AM** in cytosol, lysosomes and whole neurons of rat hippocampal slices. Indeed, the fluorescence intensity changes of cytosol and lysosomes were different, and the fluorescence intensity change of the whole neuron corresponded to the sum of those of the cytosol and lysosomes (Fig. S10b†). This may explain the low sharpness and the low S/N ratio of the fluorescence intensity changes of **CaSiR-1 AM**.

In conclusion, we utilized the 2-COOH SiR650 scaffold to develop **CaSiR-2 AM**, which shows efficient cytosolic distribution. The intramolecular spirolactone form of 2-COOH SiR650 is probably important for the cell-membrane permeability on the basis of the fluorescence imaging with 2-COOH SiR650 and two more its analogues bearing a carboxy group at the different position of the benzene moiety (Fig. S11, S12 and Table S2†). We confirmed that it can monitor $Ca^{2+}$ concentration changes in both living cells and rat brain slices with a high S/N ratio, thereby complementing conventionally used green $Ca^{2+}$ indicators, such as Oregon Green 488 BAPTA and Fluo-4.[10,12] This probe would be useful for the multicolour imaging with red and deep-red indicators. Comparison of **CaSiR-2 AM** and **CaSiR-1 AM** revealed that the latter's intracellular localization to lysosomes greatly reduces the S/N ratio in the observation of cytosolic $Ca^{2+}$ fluctuations. Our findings show that appropriate control of the intracellular localization of fluorescent indicators is extremely important to obtain good results in live-cell and tissue experiments. We expect that the design approach described here will also be applicable to the development of other activatable far-red to NIR fluorescence probes for detecting biomolecules such as NO, metal ions and so on[18,30] in cytosol.

## Conflicts of interest

There are no conflicts to declare.

## Acknowledgements

This work was supported in part by JSPS KAKENHI Grant Numbers JP20H02701, JP20H04767, JP18H04609 and JP16H05099 to K. H., JP18H05525 to Y. I. and JP16H06574 to T. U., JST ERATO (grant number: JPMJER1801) to Y. I., JST SENTAN to K. H, a grant from the Japan Agency for Medical Research and Development (AMED) to K. H. (JP18fm0208029), Hoansha Foundation to K. H. and Daiichi Sankyo Foundation of Life Science to K. H. This work was also supported by JSPS Core-to-Core Program (grant number: JPJSCCA20170007) and a Grant-in-Aid for Scientific Research on Innovative Areas "Singularity Biology (No. 8007)" (JP19H05414 to K. H.) from The Ministry of Education, Culture, Sports, Science, and Technology, Japan. K. N. was supported by a Grant-in-Aid for JSPS Fellows.

## Notes and references

1 D. E. Clapham, *Cell*, 2007, **131**, 1047.
2 M. J. Berridge, M. D. Bootman and H. L. Roderick, *Nat. Rev. Mol. Cell Biol.*, 2003, **4**, 517.
3 G. Smith, M. Reynolds, F. Burton and O. J. Kemi, *Methods Cell Biol.*, 2010, **99**, 225.
4 C. Grienberger and A. Konnerth, *Neuron*, 2012, **73**, 862.
5 W. Wang, C. K. Kim and A. Y. Ting, *Nat. Chem. Biol.*, 2019, **15**, 101.
6 M. Schäferling, *Angew. Chem., Int. Ed.*, 2012, **51**, 3532.
7 M. Oheim, M. van 't Hoff, A. Feltz, A. Zamaleeva, J. M. Mallet and M. Collot, *Biochim. Biophys. Acta*, 2014, **1843**, 2284.
8 M. Fernández-Suárez and A. Y. Ting, *Nat. Rev. Mol. Cell Biol.*, 2008, **9**, 929.
9 A. Minta, J. P. Y. Kao and R. Y. Tsien, *J. Biol. Chem.*, 1989, **264**, 8171.
10 K. R. Gee, K. A. Brown, W.-N. U. Chen, J. Bishop-Stewart and D. G. I. Johnson, *Cell Calcium*, 2000, **27**, 97.
11 Y. Lu and M. F. Paige, *J. Fluoresc.*, 2007, **17**, 739.
12 T. Sasaki, N. Matsuki and Y. Ikegaya, *Science*, 2011, **331**, 599.
13 R. Weissleder and V. Ntziachristos, *Nat. Med.*, 2003, **9**, 123.

14 J. V. Frangioni, *Curr. Opin. Chem. Biol.*, 2003, **7**, 626.
15 T. Egawa, K. Hirabayashi, Y. Koide, C. Kobayashi, N. Takahashi, T. Mineno, T. Terai, T. Ueno, T. Komatsu, Y. Ikegaya, N. Matsuki, T. Nagano and K. Hanaoka, *Angew. Chem., Int. Ed.*, 2013, **52**, 3874.
16 K. Hirabayashi, K. Hanaoka, T. Egawa, C. Kobayashi, S. Takahashi, T. Komatsu, T. Ueno, T. Terai, Y. Ikegaya, T. Nagano and Y. Urano, *Cell Calcium*, 2016, **60**, 256.
17 H. Ogasawara, M. Grzybowski, R. Hosokawa, Y. Sato, M. Taki and S. Yamaguchi, *Chem. Commun.*, 2018, **54**, 299.
18 M. Beija, C. A. M. Afonso and J. M. G. Martinho, *Chem. Soc. Rev.*, 2009, **38**, 2410.
19 T. Egawa, K. Hanaoka, Y. Koide, S. Ujita, N. Takahashi, Y. Ikegaya, N. Matsuki, T. Terai, T. Ueno, T. Komatsu and T. Nagano, *J. Am. Chem. Soc.*, 2011, **133**, 14157.
20 M. Mizunuma, H. Norimoto, K. Tao, T. Egawa, K. Hanaoka, T. Sakaguchi, H. Hioki, T. Kaneko, S. Yamaguchi, T. Nagano, N. Matsuki and Y. Ikegaya, *Nat. Neurosci.*, 2014, **17**, 503.
21 E. Kim, K. S. Yang, R. H. Kohler, J. M. Dubach, H. Mikula and R. Weissleder, *Bioconjugate Chem.*, 2015, **26**, 1513.
22 E. Kim, K. S. Yang, R. J. Giedt and R. Weissleder, *Chem. Commun.*, 2014, **50**, 4504.
23 M. A. Miller, E. Kim, M. F. Cuccarese, A. L. Plotkin, M. Prytyskach, R. H. Kohler, M. J. Pittet and R. Weissleder, *Chem. Commun.*, 2018, **54**, 42.
24 Q. Zheng, A. X. Ayala, I. Chung, A. V. Weigel, A. Ranjan, N. Falco, J. B. Grimm, A. N. Tkachuk, C. Wu, J. Lippincott-Schwartz, R. H. Singer and L. D. Lavis, *ACS Cent. Sci.*, 2019, **5**, 1602.
25 G. Lukinavičius, K. Umezawa, N. Olivier, A. Honigmann, G. Yang, T. Plass, V. Mueller, L. Reymond, I. R. Corrêa Jr., Z.-G. Luo, C. Schultz, E. A. Lemke, P. Heppenstall, C. Eggeling, S. Manley and K. Johnsson, *Nat. Chem.*, 2013, **5**, 132.
26 E. Lloyd-Evans, A. J. Morgan, X. He, D. A. Smith, E. Elliot-Smith, D. J. Sillence, G. C. Churchill, E. H. Schuchman, A. Galione and F. M. Platt, *Nat. Med.*, 2008, **14**, 1247.
27 D. M. Zhu, E. Tekle, C. Y. Huang and P. B. Chock, *J. Biol. Chem.*, 2000, **275**, 6063.
28 S. Kawano, K. Otsu, A. Kuruma, S. Shoji, E. Yanagida, Y. Muto, F. Yoshikawa, Y. Hirayama, K. Mikoshiba and T. Furuichi, *Cell Calcium*, 2006, **39**, 313.
29 D. S. Barrack, R. Thul and M. R. Owen, *J. Theor. Biol.*, 2014, **347**, 17.
30 H. Kojima, M. Hirotani, N. Nakatsubo, K. Kikuchi, Y. Urano, T. Higuchi, Y. Hirata and T. Nagano, *Anal. Chem.*, 2001, **73**, 1967.